Available online at www.sciencedirect.com
ScienceDirect
Journal of Catalysis 243 (2006) 99–107
JOURNAL OF CATALYSIS
www.elsevier.com/locate/jcat

Spontaneous catalytic activation of Ni_3Al thin foils in methanol decomposition

Dong Hyun Chun [a,b,*], Ya Xu [b], Masahiko Demura [b], Kyosuke Kishida [c], Dang Moon Wee [a], Toshiyuki Hirano [b]

[a] *Department of Materials Science and Engineering, KAIST, Daejeon 305-701, South Korea*
[b] *National Institute for Materials Science, 1-2-1 Sengen, Tsukuba, Ibaraki 305-0047, Japan*
[c] *Department of Materials Science and Engineering, Kyoto University, Kyoto 606-8501, Japan*

Received 13 May 2006; revised 28 June 2006; accepted 6 July 2006

Available online 22 August 2006

Abstract

Methanol decomposition was carried out over flat cold-rolled foils of intermetallic compound Ni_3Al in a temperature range 513–793 K. The methanol decomposition into H_2 and CO was effectively catalyzed at 713–793 K, without any need for coating catalyst layers on the foil surface before reaction. Both catalytic activity and selectivity to H_2 and CO production increased with time during the initial period of reaction, indicating that the Ni_3Al foils were spontaneously activated under the reaction conditions. Analysis of the catalytic reaction revealed that the methanol decomposition accompanied three minor side reactions: the Boudouard reaction, (reverse) water–gas shift reaction, and methanation. Surface analyses revealed that fine Ni particles dispersed on carbon nanofibers formed on the Ni_3Al foils during the reaction at 713–793 K. We attribute the high catalytic performance at 713–793 K to the gradual formation of this nanostructure.

Keywords: Intermetallic compounds and alloys; Microreactor; Methanol decomposition; Carbon nanofibers

1. Introduction

In recent years, microchanneled reactors have received much attention as compact and efficient hydrogen production systems utilizing alcohol or hydrocarbon, due to their high surface-to-volume ratio and high rates of heat and mass transfer compared with conventional reactors [1–9]. In many cases, stainless steel or silicon-based materials have been used as structural sheets, and active catalysts and porous support materials are coated on the structural sheets by complex chemical processes [1–6]. However, the lack of heat resistance in stainless steel and the poor formability and mechanical strength in silicon-based materials have limited the application range of microchanneled reactors. It is therefore necessary to develop new materials not only with high heat-resistance but also with good formability and mechanical strength. Furthermore, simplification of the complex coating process of catalyst layers is considered as an important subject in microchanneled reactor technologies.

In this respect, intermetallic compound Ni_3Al, an excellent high-temperature structural material [10,11], has considerable promise. Thus far, we have successfully developed thin foils (23 μm) of this compound by cold-rolling [12]. Because the foils have good formability after proper heat treatment [13], they can be assembled into honeycomb monoliths [14] and microchanneled reactors [15]. In addition, we recently have found high catalytic activity and selectivity for methanol decomposition into H_2 and CO in the foils [16,17]. The unusually high catalytic performance of the flat Ni_3Al foils is attributed to this catalytically active structure; that is, fine Ni particles supported on carbon nanofibers form spontaneously on the foil surface during the reaction. The results of previous studies [10–17] demonstrate that the Ni_3Al foils can be used both as catalysts and structural sheets of microchanneled reactors for hydrogen production from methanol.

In our previous study, we reported the catalytic properties for methanol decomposition at one specific temperature 793 K. In

* Corresponding author. Fax: +82 42 869 4275.
E-mail address: cdhsl@kaist.ac.kr (D.H. Chun).

0021-9517/$ – see front matter
doi:10.1016/j.jcat.2006.07.011

the present study, we report the effects of reaction temperature as well as reaction time on the catalytic reactions and evolution of surface products in a wider temperature range 513–793 K. Mechanisms of the catalytic reactions and process of activation are discussed based on the results.

2. Experimental

2.1. Sample preparation

Ni_3Al foils of 30 μm thickness were fabricated by 98% cold-rolling of single crystalline plates of Ni_3Al (Ni–24 at% Al) without intermediate annealing. Details of the foil fabrication procedure were described previously [12]. For comparison, 50-μm-thick pure Ni foils (Nilaco) were used for catalytic experiments.

2.2. Catalytic reaction

Catalytic experiments were carried out over the foil samples in a conventional fixed-bed flow reactor composed of a quartz tube, in a process similar to that described previously [16–19]. Before measurement, the samples were reduced at 513 K for 1 h in flowing hydrogen. After the hydrogen was flushed with nitrogen, methanol was introduced to the quartz tube at a liquid hourly space velocity (LHSV) of 0.0011 $m^3\,h^{-1}\,m^{-2}$ (defined as the volume of methanol passed over the unit geometrical surface area of the foil sample per hour). Methanol was fully evaporated in a thermal evaporator at 423 K before being introduced to the quartz tube. The catalytic properties of the foil samples were evaluated in a temperature range of 513–793 K by measuring the outlet composition of gaseous products with a gas chromatograph (GL Science) and the total flow rate of outlet gases with a soap bubble meter. Because the samples were in foil form, unlike common catalysts, the production rate of each gaseous product was reported in $mol\,h^{-1}\,m^{-2}$. We calculated the production rates of the gaseous products by the following equation:

$$R_{H_2} = \frac{C_{H_2} \times F_{total}}{A}, \tag{1}$$

where R_{H_2} is the production rate of H_2; C_{H_2} is the volume fraction of H_2 in total outlet gases excluding gasified species, CH_3OH and H_2O; F_{total} is the flow rate of total outlet gases ($mol\,h^{-1}$) excluding gasified species; and A is the geometrical surface area of the foil sample (0.0055 m^2). The production rates of CO, CH_4, and CO_2 were obtained using a similar calculation. The production rate of H_2O was calculated based on the ratio of volume fraction of H_2 to that of gasified H_2O in total outlet gases.

Two types of reaction tests were performed:

- *Isochonal tests*. To survey the general temperature dependence of the catalytic reactions, methanol decomposition was performed with increasing reaction temperature stepwise from 513 to 793 K at an interval of 40 K. The outlet composition and total flow rate of the gaseous products were measured after holding at each temperature for 20 min.
- *Isothermal tests*. To investigate the time dependence of the catalytic reactions, methanol decomposition was performed at isothermal conditions of 633, 713, and 793 K.

2.3. Sample characterization

The surface morphologies of the samples after the isothermal tests were observed by means of scanning electron microscopy (SEM) using a JEOL model JSM-7000F with a field emission gun. Detailed morphological investigations were performed by means of transmission electron microscopy (TEM) using a FEI Technai G2 F3 S-Twin with a field emission gun, operated at 300 kV. The composition of the surface products was analyzed by energy dispersive X-ray spectroscopy (EDS) using scanning transmission electron microscopy (STEM) with a probe size <5 nm. The crystal structures of the surface products were characterized by X-ray diffraction (XRD) with a Rigaku RINT 2500V using a Cu$K\alpha$ source. The XRD samples were collected by scraping off the surface products for precise measurement. All measurements were performed using the $\theta/2\theta$ scanning method. The Brunauer–Emmett–Teller (BET) surface areas of the samples were determined with a surface area analyzer (Quanta Chome, Autosorb) using N_2 as adsorbent. The surface area of each sample (m^2/m^2) was expressed as the measured BET surface area for the unit geometrical surface area of the foil sample.

3. Results

3.1. Isochonal tests

Catalytic performance of the cold-rolled Ni_3Al foils for methanol decomposition into H_2 and CO was surveyed at increasing reaction temperatures from 513 to 793 K, and the results were compared with those for pure Ni foils. Fig. 1 shows the production rates of H_2 and CO as a function of reaction temperature. The production rates of H_2 and CO were low below 713 K; however, they increased steeply above 713 K as the reaction temperature increased, indicating the onset of catalytic activation. In comparison, the Ni foils showed a very small increase in the production rates of both gases with increased temperature.

3.2. Isothermal tests

Because the Ni_3Al foils showed catalytic activity above 713 K, we performed isothermal tests of methanol decomposition at 633, 713, and 793 K. Fig. 2 shows the methanol conversion as a function of reaction time. The methanol conversion increased with increased reaction time at all reaction temperatures, indicating that the cold-rolled Ni_3Al foils were spontaneously activated during the tests. The spontaneous activation occurred more favorably at higher reaction temperatures. At 793 K, methanol conversion increased rapidly with

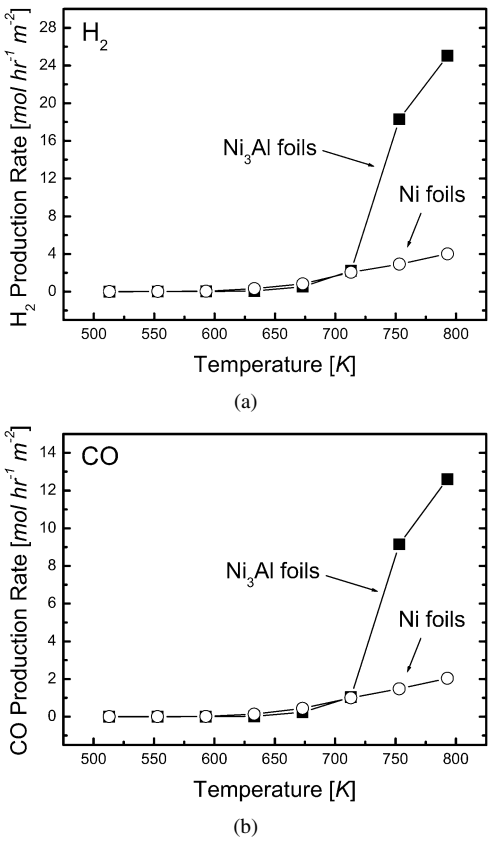

Fig. 1. Production rates of (a) H_2 and (b) CO in methanol decomposition over Ni_3Al foils as a function of reaction temperature. For comparison, the result over Ni foils is inserted.

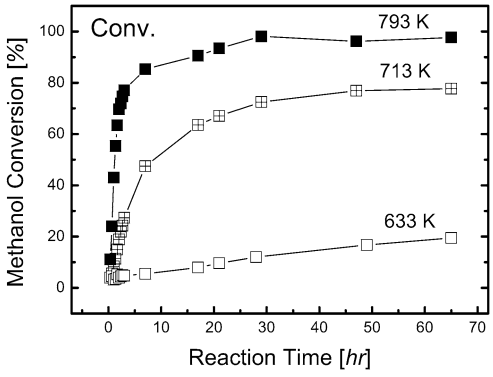

Fig. 2. Methanol conversion over Ni_3Al foils at 633, 713, and 793 K as a function of reaction time.

increasing reaction time during the first several hours, reaching a steady-state value of about 98% after 29 h of reaction, as we previously reported [16]. No considerable change occurred thereafter. Methanol conversion showed a similar tendency at 713 and 633 K; however, both the initial increasing rate and the steady-state value were low at these temperatures compared with those at 793 K.

Fig. 3 shows the production rates of outlet gases as a function of reaction time, as we previously reported [17]. As shown in Figs. 3a and 3b, the production rates of H_2 and CO were much higher than those of other gases for all conditions, and thus the main reaction was

$$CH_3OH(g) \rightleftarrows CO(g) + 2H_2(g). \quad (2)$$

Both production rates increased with increased reaction time and temperature, corresponding to the methanol conversion, as shown in Fig. 2. This behavior is quite different from that of common Ni catalysts for methanol decomposition. For example, for Ni/SiO_2 catalysts, methanol initially decomposes into H_2 and CO, but methanation of CO soon follows via the consumption of H_2. As a result, the main products are CH_4, CO_2, and H_2O [20]. Fig. 4 shows that the ratio of both production rates is higher than the stoichiometric value of Eq. (2) at the initial reaction period ($H_2/CO = 2.0$), and that it decreases to the stoichiometric value with increased reaction time.

Small amounts of H_2O, CH_4, and CO_2 were also produced along with to the main products, as shown in Figs. 3c–3e. Note the difference in the vertical scale between Figs. 3a and 3b and Figs. 3c–3e. The production rates of these minor products generally increased with increasing temperature and time, but the time dependence was different from that for methanol conversion, particularly at 793 K. The production rate of H_2O increased rapidly with increased time at the beginning of the reaction (Fig. 3c), then decreased slightly and gradually increased again, showing a local maximum and minimum. In contrast, the production rates of CH_4 and CO_2 increased gradually and continuously with increased time even after the methanol conversion reached almost 100% (after 29 h). Nevertheless, the production rate of CH_4 was extremely low compared with that over Ni/SiO_2 catalysts. (CH_4 is the major product of methanol decomposition over Ni/SiO_2 catalysts [20].)

3.3. Surface characterization after isothermal tests

Before the reaction, the foil surface was macroscopically smooth with a shiny metallic luster, but had a rolling deformation structure [21]. After the isothermal tests at all reaction temperatures, the surface was covered in soot due to deposition of carbon during the reaction. Surface observation by SEM (Fig. 5) revealed a drastic evolution of reaction products during the reaction. At 793 K, small Ni particles (<250 nm in diameter) formed on the foil surface after 1 h of reaction (Fig. 5i). After 2 h of reaction, carbon nanofibers formed (Fig. 5j). Both the Ni particles and the carbon nanofibers were identified by TEM and XRD. The Ni particles were dispersed on the carbon nanofibers. The size of the particles corresponded closely with the diameter of the carbon nanofibers. The number of both products significantly increased over the entire surface of the foils with increasing reaction time (Figs. 5j–5l). After 7 h of reaction, most of the Ni particles were <100 nm in diameter, as we reported previously [16]. After 65 h of reaction, the particle size ranged from several tens to hundreds of nanometers in diameter. The particles <100 nm in diameter tended to be located at the top of the carbon nanofibers, and those >100 nm in diameter tended to be located on the middle region of the fibers. At 713 K, Ni particles also formed after 1 h of reaction (shown by arrows in Figs. 5e and 5f). However, the particles were sparsely distributed and small compared with those at 793 K. Blocky products were observed at this stage but remained unidentified.

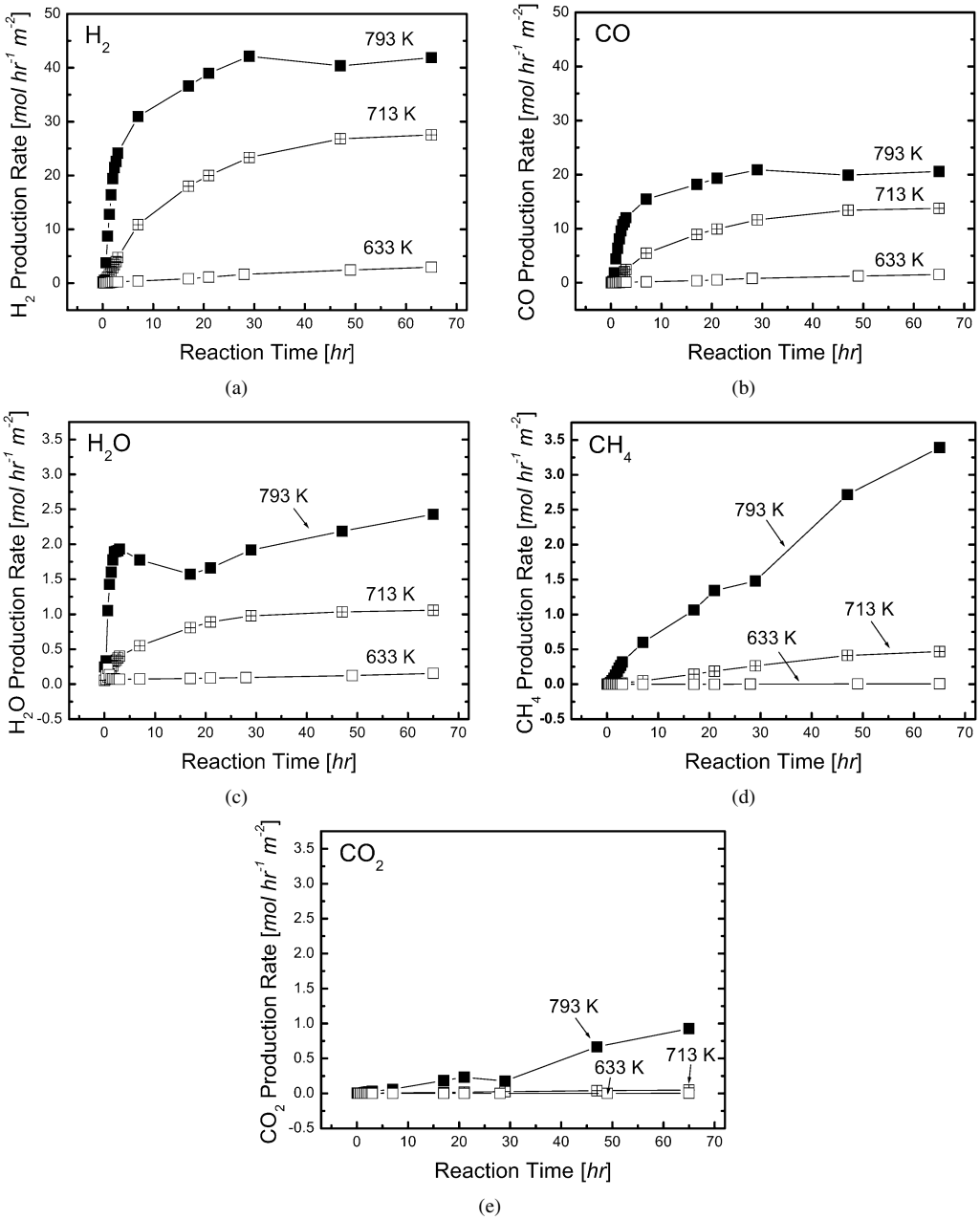

Fig. 3. Production rates of (a) H_2, (b) CO, (c) H_2O, (d) CH_4, and (e) CO_2 in methanol decomposition over Ni_3Al foils at 633, 713, and 793 K as a function of reaction time.

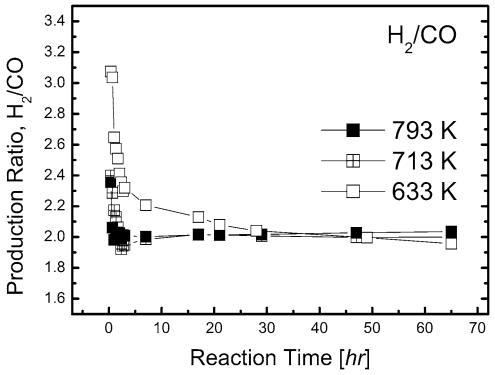

Fig. 4. Ratio of H_2 to CO production in methanol decomposition over Ni_3Al foils at 633, 713, and 793 K as a function of reaction time.

Formation of carbon nanofibers was slow compared to that at 793 K; specifically, nanofibers formed after 7 h of reaction. After 65 h of reaction, there was no difference in the size and distribution of either the Ni particles or the carbon nanofibers between 713 and 793 K (Figs. 5h and 5l). At 633 K, formation of reaction products was quite slow. The amount of Ni particles was negligible until 7 h of reaction, and no carbon nanofiber was observed on the surface though the whole range of reaction time (Figs. 5a–5d).

A detailed surface structure analysis was performed on the foil after 1 h of reaction at 793 K (Fig. 5i) using TEM and STEM-EDS, as shown in Fig. 6. The cross-sectional TEM image shows the formation of a small particle and a thin layer on the foils. The elemental mapping by STEM-EDS revealed

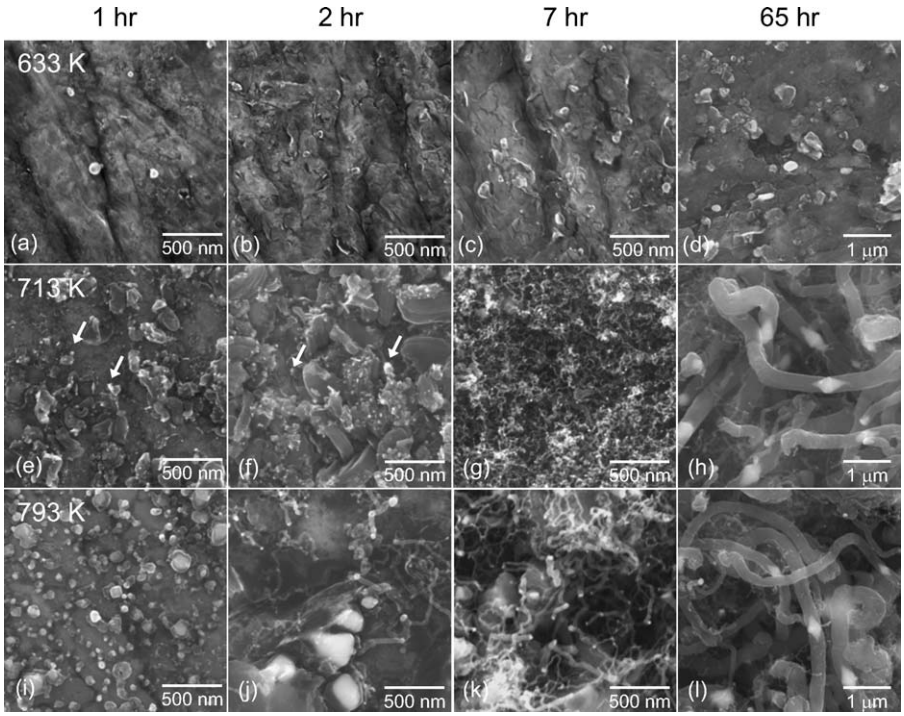

Fig. 5. Surface SEM images of Ni_3Al foils after (a, e, i) 1 h, (b, f, j) 2 h, (c, g, k) 7 h, and (d, h, l) 65 h of reaction at (a–d) 633 K, (e–h) 713 K, and (i–l) 793 K.

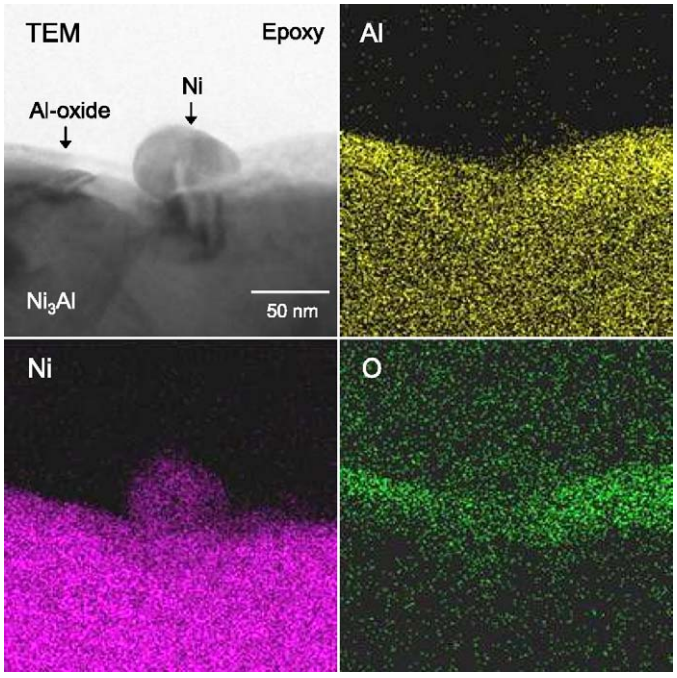

Fig. 6. Cross-sectional TEM image and corresponding elemental mapping by STEM-EDS for Ni_3Al foils after 1 h of reaction at 793 K.

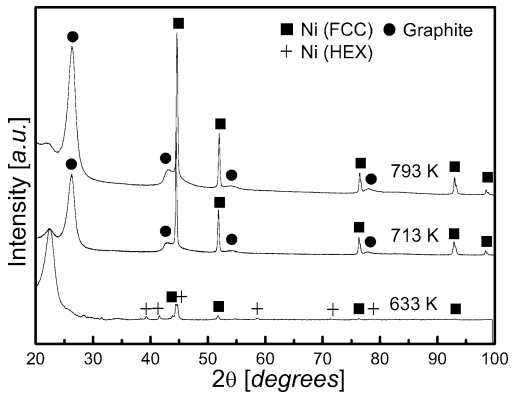

Fig. 7. XRD patterns for surface products on Ni_3Al foils after 65 h of reaction at 633, 713, and 793 K.

that the particles contained mainly Ni and almost no Al and O, thus confirming the formation of small Ni particles on the surface at the beginning of the reaction. The thin layer contained mainly Al and O, indicating the formation of Al-oxide, which agrees well with our previously reported XPS results [16] that Al in the Ni_3Al foils was selectively oxidized and hydroxylated during methanol decomposition. As we previously discussed, selective oxidation and/or hydroxylation of Al in the Ni_3Al foils is thought to leave Ni atoms behind, resulting in aggregation into small Ni particles. The small Ni particles can serve as effective catalysts for methanol decomposition.

The crystal structures of the surface products after 65 h of reaction were characterized by XRD, as shown in Fig. 7. The XRD patterns confirmed the formation of graphite and metallic Ni at 713 and 793 K, which are often reported in Ni particles supported on carbon nanofibers [22,23]. In contrast, the XRD patterns showed the formation of metallic Ni and no graphite at 633 K, indicating that the carbon produced was likely amorphous.

Surface areas of the samples before and after 65 h of reaction are given in Table 1. The surface area before reaction was approximately 17 m^2/m^2. Therefore, the BET surface area of the cold-rolled Ni_3Al foils is roughly 17 times greater than the geo-

Table 1
Surface area (m^2/m^2) of Ni_3Al foils before and after 65 h of reaction at 633, 713, and 793 K. The surface area was obtained by normalizing the BET surface area (m^2) into the geometrical surface area (m^2)

Before reaction (m^2/m^2)	After 65 h of reaction (m^2/m^2)		
	633 K	713 K	793 K
16.6	245.6	1959.1	1711.3

metrical value, possibly due to the deformation structure. After reaction at 713 and 793 K, the surface area increased significantly, to about 1960 and 1710 m^2/m^2, respectively; thus, the surface area was 118 and 104 times larger, respectively, than the value before the reaction. The remarkable increase in surface area after reaction at 713 and 793 K is clearly due to the formation of the surface products, consisting of small Ni particles and carbon nanofibers. Notably, the increase in surface area after the reaction at 633 K was small compared with that at 713 and 793 K.

4. Discussion

4.1. Reaction system

In our previous studies, we reported the catalytic properties for methanol decomposition at one specific temperature, 793 K. In the present study, the temperature dependence of the catalytic properties became clear. The results reveal that methanol was largely decomposed into H_2 and CO over cold-rolled Ni_3Al foils above 713 K, and that the amount of product gases increased with increased reaction time. Small amounts of CH_4, CO_2, H_2O, and solid-phase carbon were also produced as byproducts, but their production was significantly suppressed compared with that of common Ni catalysts. The results indicate that our reaction system cannot be described simply by the single stoichiometric reaction of Eq. (2). Several reactions must proceed simultaneously or consecutively. In this section, we discuss the possible mechanism in terms of catalytic reaction.

Selectivity of each reaction product in the reforming process of hydrocarbon has been calculated for the case without carbon deposition on the catalyst; that is, a complete carbon balance is obtained between the feed and effluent gases [24,25]. In our previous study, we neglected carbon deposition for the calculation of selectivity in the methanol decomposition over cold-rolled Ni_3Al foils [16]. However, a small amount of solid-phase carbon formed in the form of carbon nanofibers or amorphous carbon on the foil surface (Figs. 5 and 7). Thus, it is reasonable to take into account carbon deposition when calculating selectivity. However, measuring the production rate of carbon as a function of reaction time is not easy, and thus we alternatively estimated the rate based on the following assumption.

We propose the following three reactions proceed as side reactions in addition to the main reaction (Eq. (2)). Thus, the reaction system can be written as a combination of Eqs. (2)–(5):

$$2CO(g) \rightleftarrows C(s) + CO_2(g), \tag{3}$$

$$CO_2(g) + H_2(g) \rightleftarrows CO(g) + H_2O(g), \tag{4}$$

$$CO(g) + 3H_2(g) \rightleftarrows CH_4(g) + H_2O(g). \tag{5}$$

Equations (3), (4), and (5) are referred to as Boudouard reaction, reverse water–gas shift reaction, and methanation, respectively.

Assuming the four stoichiometric reactions (Eqs. (2)–(5)), the production rate of carbon can be estimated simply by calculating the balance of the reactants and products as

$$R_C = R_{CO_2} + R_{H_2O} - R_{CH_4}, \tag{6}$$

where R_{CO_2}, R_{H_2O}, and R_{CH_4} are the experimentally measured production rates of CO_2, H_2O, and CH_4, respectively (Fig. 3). The detailed calculation procedure is described in Appendix A. Selectivities of H_2 (S_{H_2}) and the other carbon-containing reaction product, x, (S_x) can be calculated from the production rates of the products according to Cortright et al. [25] as

$$S_{H_2} = \frac{R_{H_2}}{R_{CO} + R_{CH_4} + R_{CO_2} + R_C} \times \frac{1}{RR} \times 100, \tag{7}$$

$$S_x = \frac{R_x}{R_{CO} + R_{CH_4} + R_{CO_2} + R_C} \times 100, \tag{8}$$

where R_{H_2} is the experimentally measured production rate of H_2 (Fig. 3) and RR is the H_2/CO ratio in Eq. (2); the RR value for methanol decomposition is 2.

Using Eqs. (7) and (8), the selectivities to H_2 and CO production were calculated and plotted as a function of reaction time in Fig. 8. Both selectivities were low at the beginning of the reaction, particularly at the lower reaction temperatures. After the initial period, both selectivities increased with time, eventually reaching steady-state values of around 90% at all reaction temperatures. The increase of the selectivities was rapid at 713 K and above. At 793 K, both selectivities decreased slightly after 29 h of reaction when the methanol conversion reached almost 100%. However, they remained at high, >80%, even after 65 h of reaction. Our results confirm that methanol decomposition into H_2 and CO (Eq. (2)) was the main reaction in the whole range of reaction temperatures and time in this study.

The selectivities to the production of minor components, C, CH_4, and CO_2, are shown in Fig. 9. The selectivity to C production was high at the beginning, particularly at lower temperatures, and decreased with time (Fig. 9a). At 793 K, selectivity to C production decreased to almost zero after 29 h of reaction when the methanol conversion reached almost 100%. This means that Boudouard reaction, as given in Eq. (3), occurred during the initial period of reaction. Occurrence of the Boudouard reaction may lead to the consumption of CO produced via the main reaction (Eq. (2)), resulting in a higher ratio of H_2 to CO production than the stoichiometric value during the initial period of reaction (Fig. 4). In contrast, the selectivity to CH_4 production increased gradually with increased reaction time, as shown in Fig. 9b, indicating that methanation (Eq. (5)) proceeded gradually over time. The selectivity to CO_2 production in Fig. 9c showed a similar tendency to that of C production at the initial period, that is, rapid decrease with time. However, it again increased gradually at a later period.

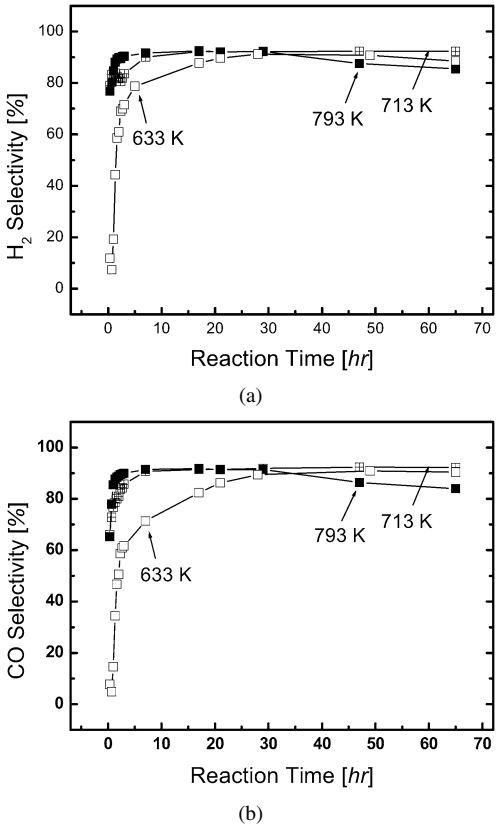

Fig. 8. Selectivities to (a) H_2 and (b) CO production in methanol decomposition over Ni_3Al foils at 633, 713, and 793 K as a function of reaction time.

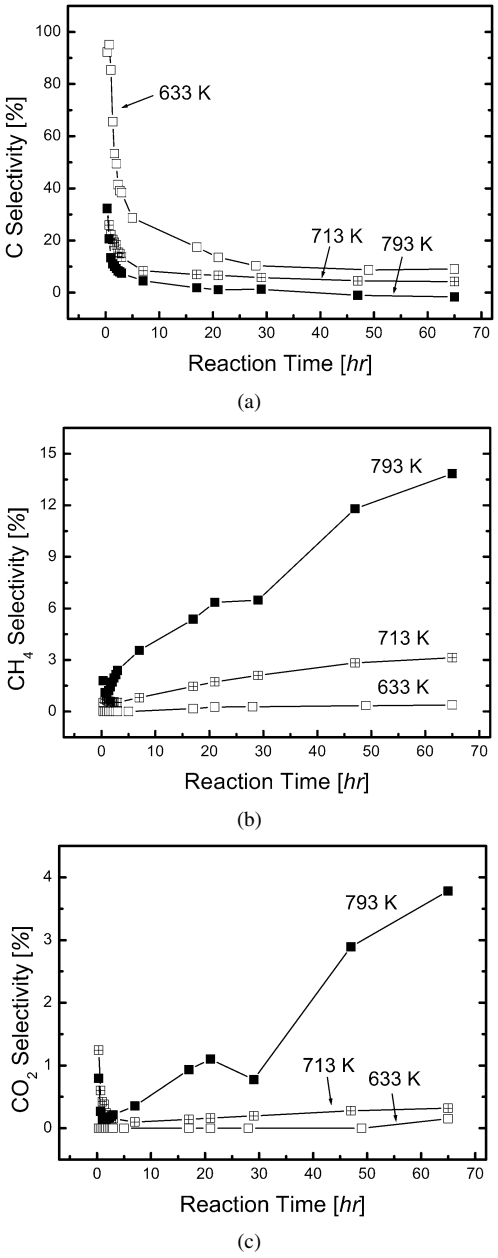

Fig. 9. Selectivities to (a) C, (b) CH_4, and (c) CO_2 production in methanol decomposition over Ni_3Al foils at 633, 713, and 793 K as a function of reaction time.

Considering that the selectivity of CO_2 was much lower than that of C in the initial period, CO_2 is likely produced via a Boudouard reaction (Eq. (3)) and consumed via a reverse water–gas shift reaction (Eq. (4)) at the initial period; that is, the initial period can be described by a combination of Eqs. (2), (3), and (4). On the other hand, because the selectivity to CO_2 production increased gradually at the later period, even after the Boudouard reaction (Eq. (3)) was terminated, the water–gas shift reaction (the reverse reaction of Eq. (4)) appears to have occurred with the progression of methanation (Eq. (5)) after the initial period. Thus, the reaction system at the later period can be described by a combination of Eqs. (2), (4), and (5). According to these considerations, the change in H_2O production rate, as given in Fig. 3c, also can be adequately described.

Based on these analyses, we suggest that the methanol decomposition over cold-rolled Ni_3Al foils proceeded mainly via the process described in Eq. (2), accompanying three minor side reactions (Eqs. (3)–(5)). Among the side reactions, the Boudouard reaction (Eq. (3)) and the reverse water–gas shift reaction (Eq. (4)) occurred preferentially during the initial period, and methanation (Eq. (5)) followed thereafter with the water–gas shift reaction (the reverse reaction of Eq. (4)).

4.2. Activation process

As shown in Figs. 3 and 8, both the activity and the selectivity to H_2 production increased rapidly during the initial period of reaction above 713 K. This rapid increase is favorable in terms of practical applications, demonstrating that efficient hydrogen production is possible using flat foils without the need for a complex coating process of the catalyst layers. In our previous study [16], we pointed out that the high catalytic activity can be attributed to the spontaneous formation of fine Ni particles dispersed on the carbon nanofibers.

Fine Ni particles are known to be active catalysts for methanol decomposition [20,26–30]. We consider this to hold true in the present study, as the increase in the number of Ni particles led to increased catalytic activity with increased reaction time. We have previously discussed the formation mechanism of fine Ni particles during the reaction based on the results of XPS analyses [16]; that is, Al in the Ni_3Al foils is selectively

oxidized and hydroxylated to form Al_2O_3 and $Al(OH)_3$ during the initial period of reaction. This oxidation mechanism may involve the following reactions:

$$2Al(s) + 3H_2O(g) \rightleftarrows Al_2O_3(s) + 3H_2(g) \quad (9)$$

and

$$2Al(s) + 6H_2O(g) \rightleftarrows 2Al(OH)_3(s) + 3H_2(g). \quad (10)$$

The selective oxidation and hydroxylation of Al can lead to the formation of fine Ni particles, possibly because Ni atoms remain and aggregate into fine Ni particles. In this study, we confirmed by TEM observation that fine Ni particles and Al-oxide formed at the beginning of the reaction (Fig. 6). Considering that H_2 and CO were the major products, the reaction atmosphere must have been highly reducing. However, because a small amount of H_2O was also produced via the reverse water–gas shift reaction (Eq. (4)) and/or methanation (Eq. (5), Fig. 3c), the oxygen partial pressure in the reaction atmosphere is considered low, in the range where Al_2O_3 and $Al(OH)_3$ can form selectively. The observation that fine Ni particles were favorably produced at 713 K and above (Fig. 5) indicates that this mechanism works effectively at high temperatures. Several researchers have reported a similar mechanism for the oxidation of Ni_3Al under low oxygen partial pressures [31–33]. They found that pure metallic Ni particles and Al_2O_3 formed above 773 K as a result of selective oxidation of Al in Ni_3Al, which is basically consistent with the mechanism described in the present study.

Carbon nanofibers are effective potential catalyst supports because of their high surface area with a large number of edges [34]. This characteristic surface is favorable for high catalytic performance because fine catalyst particles can be highly dispersed on the surface. Normally, carbon nanofibers are produced by the catalytic decomposition of hydrocarbon gases or carbon monoxide over selected metal particles, such as Fe, Co, and Ni, in a temperature range 673–1273 K [35,36]. In particular, in the temperature range 773–873 K, carbon nanofibers are more favorably produced over other types of carbon deposits, such as amorphous or graphitic carbons. In this study, carbon nanofibers formed above 713 K and amorphous carbon formed below 713 K (Figs. 5 and 7), which is consistent with previous reports [35,36]. The manner of carbon deposition is coincident with the formation of fine Ni particles; fine Ni particles formed densely above 713 K on the surface of carbon nanofibers.

We consider the formation of fine Ni particles and carbon nanofibers a coupled phenomenon, as illustrated in Fig. 10. First, fine Ni particles form as a result of selective oxidation and hydroxylation of Al, as described above. Then, formation of solid-phase carbon proceeds over the Ni particles via the Boudouard reaction (Eq. (3)). The deposited carbon possibly diffuses to grow in the form of a fibrous structure above 713 K, maintaining Ni particle surfaces that are free of deposited carbon, as previously proposed [35,36]. The produced carbon nanofibers are considered to suppress the coalescence of the Ni particles, acting as a means of support for heterogeneous catalysts [22,23,34]. These mechanisms may contribute to maintaining the catalytic activity and selectivity of the Ni particles during the reaction.

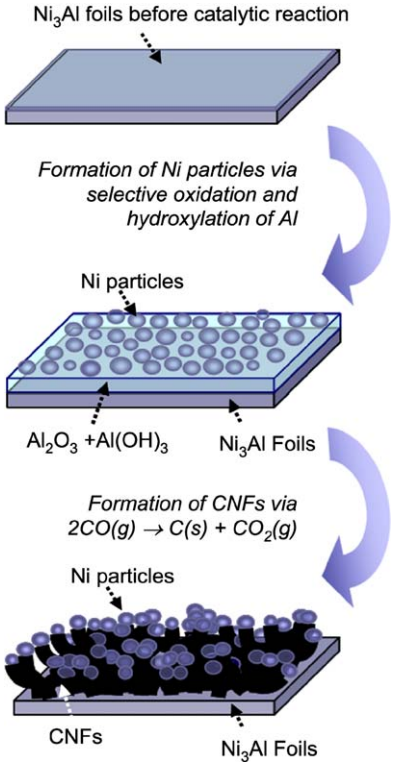

Fig. 10. Schematic diagram for spontaneous activation process of Ni_3Al foils during the reaction at 713–793 K.

5. Conclusion

Catalytic properties of intermetallic compound Ni_3Al foils for methanol decomposition were evaluated at various reaction temperatures ranging from 513 to 793 K. Our main results can be summarized as follows:

(1) Ni_3Al foils demonstrated high catalytic activity for methanol decomposition into H_2 and CO in a temperature range 713–793 K but low catalytic activity below 713 K.
(2) Both the catalytic activity and selectivity to H_2 and CO production increased with increasing time during the initial period of reaction and became stable during the subsequent reaction.
(3) The main reaction, methanol decomposition into H_2 and CO (Eq. (2)), accompanied three minor side reactions: the Boudouard reaction (Eq. (3)), the reverse water–gas shift reaction (Eq. (4)), and methanation (Eq. (5)). Among the side reactions, the process described in Eqs. (3) and (4) occurred preferentially during the initial period, and that of Eq. (5) followed thereafter, accompanying the reverse reaction of Eq. (4).
(4) Fine Ni particles dispersed on carbon nanofibers formed spontaneously on the foil surface at 713 K and above during the reaction. The rapid increase in the catalytic activity with increased time at 713–793 K is attributed to the spontaneous formation of this nanostructure.

Acknowledgments

This work was supported in part by the Korea Science and Engineering Foundation (KOSEF-R01-2003-000-10433-0), the Korea Research Foundation Grant funded by the Korean government (MOEHD) (KRF-2005-213-D00038), and the Iketani Science and Technology Foundation, Japan.

Appendix A

We estimated the production rate of solid-phase carbon by calculating the balance of the reactants and products appearing in three reactions (Eqs. (3)–(5)). The detailed procedures are as follows:

First, we assume that

$$R_{\mathrm{CO_2(Eq.\,(3))}} = R_{\mathrm{C(Eq.\,(3))}} = R_{\mathrm{C(total)}}, \tag{A.1}$$

where $R_{\mathrm{CO_2(Eq.\,(3))}}$ and $R_{\mathrm{C(Eq.\,(3))}}$ are the production rates of CO_2 and C via Eq. (3), respectively, and $R_{\mathrm{C(total)}}$ is the total production rate of C (estimated value). In the same way, we assume that

$$R_{\mathrm{CO_2(Eq.\,(4))}} = R_{\mathrm{H_2O(Eq.\,(4))}} = R_{\mathrm{H_2O(total)}} - R_{\mathrm{H_2O(Eq.\,(5))}}, \tag{A.2}$$

where $R_{\mathrm{CO_2(Eq.\,(4))}}$ and $R_{\mathrm{H_2O(Eq.\,(4))}}$ are the consuming rate of CO_2 and the production rate of H_2O via Eq. (4), respectively, $R_{\mathrm{H_2O(total)}}$ is the total production rate of H_2O (measured value), and $R_{\mathrm{H_2O(Eq.\,(5))}}$ is the production rate of H_2O via Eq. (5). Also, we assume that

$$R_{\mathrm{CH_4(Eq.\,(5))}} = R_{\mathrm{H_2O(Eq.\,(5))}} = R_{\mathrm{CH_4(total)}}, \tag{A.3}$$

where $R_{\mathrm{CH_4(Eq.\,(5))}}$ is the production rate of CH_4 via Eq. (5) and $R_{\mathrm{CH_4(total)}}$ is the total production rate of CH_4 (measured value). Furthermore, we assume that

$$R_{\mathrm{CO_2(total)}} = R_{\mathrm{CO_2(Eq.\,(3))}} - R_{\mathrm{CO_2(Eq.\,(4))}} \tag{A.4}$$

from Eqs. (3) and (4), where $R_{\mathrm{CO_2(total)}}$ is the total production rate of CO_2 (measured value). Finally, we can derive the total production rate of C as a function of the total production rates of CO_2, H_2O, and CH_4 from Eqs. (A.1)–(A.4) as

$$R_{\mathrm{C(total)}} = R_{\mathrm{CO_2(total)}} + R_{\mathrm{H_2O(total)}} - R_{\mathrm{CH_4(total)}}. \tag{A.5}$$

References

[1] M.T. Janicke, H. Kestenbaum, U. Hagendorf, F. Schüth, M. Fichtner, K. Schubert, J. Catal. 191 (2000) 282.
[2] X. Yu, S.T. Tu, Z. Wang, Y. Qi, Chem. Eng. J. 116 (2006) 123.
[3] J.Y. Won, H.K. Jun, M.K. Jeon, S.I. Woo, Catal. Today 111 (2006) 158.
[4] Y. Kawamura, N. Ogura, T. Yamamoto, A. Igarashi, Chem. Eng. Sci. 61 (2006) 1092.
[5] R.M. Tiggelaar, P.W.H. Loeters, P. Male, R.E. Oosterbroek, J.G.E. Gardeniers, M.H.J.M. Croon, J.C. Schouten, M.C. Elwenspoek, A. Berg, Sens. Actuat. A Phys. 112 (2004) 267.
[6] R.M. Tiggelaar, P. Male, J.W. Berenschot, J.G.E. Gardeniers, R.E. Oosterbroek, M.H.J.M. Croon, J.C. Schouten, A. Berg, M.C. Elwenspoek, Sens. Actuat. A Phys. 119 (2005) 196.
[7] A.S. Bodke, S.S. Bharadwaj, L.D. Schmidt, J. Catal. 179 (1998) 138.
[8] I. Aartun, H.J. Venvik, A. Holmen, P. Pfeifer, O. Görke, K. Schubert, Catal. Today 110 (2005) 98.
[9] E.C. Wanat, B. Suman, L.D. Schmidt, J. Catal. 235 (2005) 18.
[10] N.S. Stoloff, C.T. Liu, S.C. Deevi, Intermetallics 8 (2000) 1313.
[11] N.S. Stoloff, Int. Mater. Rev. 34 (1989) 153.
[12] M. Demura, K. Kishida, Y. Suga, M. Takanashi, T. Hirano, Scr. Mater. 47 (2002) 267.
[13] C. Cui, M. Demura, K. Kishida, T. Hirano, J. Mater. Res. 20 (2005) 1054.
[14] K. Kishida, M. Demura, S. Kobayashi, Y. Xu, T. Hirano, Defect. Diffus. Forum 233–234 (2004) 37.
[15] B.K. Paul, H. Hasan, T. Dewey, D. Alman, R.D. Wilson, in: C. Mavroidis, P.S. Shiakolas, C.A. Moore, N. Sarkar, J.E. Speich (Eds.), Proc. IMECE 2002, New Orleans, Louisiana, 17–22 November, 2002, ASME, New York, 2002, pp. 32,892–32,897.
[16] D.H. Chun, Y. Xu, M. Demura, K. Kishida, M.H. Oh, T. Hirano, D.M. Wee, Catal. Lett. 106 (2006) 71.
[17] D.H. Chun, Y. Xu, M. Demura, K. Kishida, M.C. Kim, M.H. Oh, T. Hirano, D.M. Wee, J. Kor. Inst. Met. Mater. 43 (2005) 801.
[18] Y. Xu, S. Kameoka, K. Kishida, M. Demura, A.P. Tsai, T. Hirano, Intermetallics 13 (2005) 151.
[19] Y. Xu, S. Kameoka, K. Kishida, M. Demura, A.P. Tsai, T. Hirano, Mater. Trans. 45 (2004) 3177.
[20] P.K. de Bokx, A.R. Balkende, J.W. Geus, J. Catal. 117 (1989) 467.
[21] K. Kishida, M. Demura, T. Hirano, Y. Suga, in: S. Hanada, Z. Zhong, S.W. Nam, R.N. Wright (Eds.), Proc. PRICM4, Hawaii, Honolulu, 11–15 December, 2001, JIM, Sendai, 2001, pp. 867–870.
[22] K. Otsuka, H. Ogihara, S. Takenaka, Carbon 41 (2003) 223.
[23] S. Takenaka, E. Kato, Y. Tomikubo, K. Otsuka, J. Catal. 219 (2003) 176.
[24] G.W. Huber, J.W. Shabaker, J.A. Dumesic, Science 300 (2003) 2075.
[25] R.D. Cortright, R.R. Davda, J.A. Dumesic, Nature 418 (2002) 964.
[26] A.R. Balkenede, P.K. de Bokx, J.W. Geus, Appl. Catal. 30 (1987) 47.
[27] K. Nakagawa, T. Hashida, C. Kajita, N. Ikenaga, T. Kobayashi, M. Nishitani-Gamo, T. Suzuki, T. Ando, Catal. Lett. 80 (2002) 161.
[28] Y. Matsumura, N. Tode, T. Yazawa, M. Haruta, J. Mol. Catal. A Chem. 99 (1995) 183.
[29] Y. Matsumura, K. Kuraoka, T. Yazawa, M. Haruta, Catal. Today 45 (1998) 191.
[30] Y. Matsumura, K. Tanaka, N. Tode, T. Yazawa, M. Haruta, J. Mol. Catal. A Chem. 152 (2000) 157.
[31] M. Haerig, S. Hofmann, Appl. Surf. Sci. 125 (1998) 99.
[32] E. Schumann, G. Schnotz, K.P. Trumble, M. Rühle, Acta Met. Mater. 40 (1992) 1311.
[33] W. Gao, Z. Li, Z. Wu, S. Li, Y. He, Intermetallics 10 (2002) 263.
[34] N.M. Rodriguez, M.S. Kim, R.T.K. Baker, J. Phys. Chem. 98 (1994) 13,108.
[35] R.T.K. Baker, Encyclopedia of Materials: Science and Technology, Elsevier, St. Louis, 1999, pp. 932–941.
[36] R.T.K. Baker, Am. Chem. Soc. Fuel Chem. 41 (2) (1996) 521.